LEARNING TO PLAN IN HIGH DIMENSIONS VIA NEURAL EXPLORATION-EXPLOITATION TREES

Anonymous authors
Paper under double-blind review

ABSTRACT

We propose a meta path planning algorithm named *Neural Exploration-Exploitation Trees (NEXT)* for learning from prior experience for solving new path planning problems in high dimensional continuous state and action spaces. Compared to more classical sampling-based methods like RRT, our approach achieves much better sample efficiency in high-dimensions and can benefit from prior experience of planning in similar environments. More specifically, NEXT exploits a novel neural architecture which can learn promising search directions from problem structures. The learned prior is then integrated into a UCB-type algorithm to achieve an online balance between *exploration* and *exploitation* when solving a new problem. We conduct thorough experiments to show that NEXT accomplishes new planning problems with more compact search trees and significantly outperforms state-of-the-art methods on several benchmarks.

1 INTRODUCTION

Path planning is a fundamental problem with many real-world applications, such as robot manipulation and autonomous driving. A simple planning problem within low-dimensional state space can be solved by first discretizing the continuous state space into a grid, and then searching for a path on top of it using graph search algorithms such as A^* (Hart et al., 1968). However, due to the curse of dimensionality, these approaches do not scale well with the number of dimensions of the state space. For *high-dimensional* planning problems, people often resort to sampling-based approaches to avoid explicit discretization. Sampling-based planning algorithms, such as probabilistic roadmaps (PRM) (Kavraki et al., 1996), rapidly-exploring random trees (RRT) (LaValle, 1998), and their variants (Karaman & Frazzoli, 2011) incrementally build an implicit representation of the state space using probing samples. These generic algorithms typically employ a uniform sampler which does not make use of the structures of the problem. Therefore they may require lots of samples to obtain a feasible solution for complicated problems. To improve the sample efficiency, heuristic biased samplers, such as Gaussian sampler (Boor et al., 1999), bridge test (Hsu et al., 2003) and reachability-guided sampler (Shkolnik et al., 2009) have been proposed. All these sampling heuristics are designed manually to address specific structural properties, which may or may not be valid for a new problem, and may lead to even worse performance compared to the uniform proposal.

Online adaptation in path planning has also been investigated for improving sample efficiency in current planning problem. Specifically, Hsu et al. (2005) exploits online algorithms to dynamically adapts the mixture weights of several manually designed biased samplers. Burns & Brock (2005a;b) fit a model for the planning environment incrementally and use the model for planning. Yee et al. (2016) mimics the Monte-Carlos tree search (MCTS) for problems with continuous state and action spaces. These algorithms treat each planning problem *independently*, and the collected data from previous experiences and built model will be simply discarded when solving a new problem. However, in practice, similar planning problems may be solved again and again, where the problems are different but sharing common structures. For instance, grabbing a coffee cup on a table at different time are different problems, since the layout of paper and pens, the position and orientation of coffee cups may be different every time; however, all these problems show common structures of handling similar objects which are placed in similar fashions. Intuitively, if the common characteristics across problems can be learned via some shared latent representation, a planner based on such representation can then be transferred to new problems with improved sample efficiency.

Several methods have been proposed recently to learn from past planning experiences to conduct more efficient and generalizable planning for future problems. These works are limited in one way

or the other. Zucker et al. (2008); Zhang et al. (2018); Huh & Lee (2018) treat the sampler in the sampling-based planner as a stochastic policy to be learned and apply policy gradient or TD-algorithm to improve the policy. Finney et al. (2007); Bowen & Alterovitz (2014); Ye & Alterovitz (2017); Ichter et al. (2018); Kim et al. (2018); Kuo et al. (2018) apply imitation learning based on the collected demonstrations to bias for better sampler via variants of probabilistic models, *e.g.*, (mixture of) Gaussians, conditional VAE, GAN, HMM and RNN. However, many of these approaches either rely on specially designed local features or assume the problems are indexed by special parameters, which limits the generalization ability. Deep representation learning provides a promising direction to extract the common structure among the planning problems, and thus mitigate such limitation on hand-designed features. However, existing work, *e.g.*, motion planning networks (Qureshi et al., 2019), value iteration networks (VIN) (Tamar et al., 2016), and gated path planning networks (GPPN) (Lee et al., 2018), either apply off-the-shelf MLP architecture ignoring special structures in planning problems or can only deal with discrete state and action spaces in low-dimensional settings.

In this paper, we present *Neural EXploration-EXploitation Tree (NEXT)*, a **meta neural path planning** algorithm for high-dimensional continuous state space problems. The core contribution is a novel **attention-based neural architecture** that is capable of learning generalizable problem structures from previous experiences and produce promising search directions with automatic online **exploration-exploitation** balance adaption. Compared to existing learning-based planners,

- **NEXT is more generic**. We propose an architecture that can embed high dimensional continuous state spaces into low dimensional discrete spaces, on which a neural planning module is used to extract planning representation. These module will be learned end-to-end.
- **NEXT balances exploration-exploitation trade-off**. We integrate the learned neural prior into an upper confidence bound (UCB) style algorithm to achieve an online balance between exploration and exploitation when solving a new problem.

Empirically, we show that NEXT can exploit past experiences to reduce the number of required samples drastically for solving new planning problems, and significantly outperforms previous state-of-the-arts on several benchmark tasks.

1.1 Related Works

Designing non-uniform sampling strategies for random search to improve the planning efficiency has been considered as we discussed above. Besides the mentioned algorithms, there are other works along this line, including informed RRT* (Gammell et al., 2014) and batch informed Trees (BIT*) (Gammell et al., 2015) as the representative work. Randomized A^* (Diankov & Kuffner, 2007) and Sampling-based A^* (Persson & Sharf, 2014) expand the search tree with hand-designed heuristics. These methods incorporate the human prior knowledge via hard-coded rules, which is fixed and unable to adapt to problems, and thus, may not universally applicable. Bhardwaj et al. (2017) attempts to learn such heuristics. However, their method is restricted to planning on graphs.

The online exploration-exploitation trade-off is also an important issue in planning. For instance, Rickert et al. (2009) constructs a potential field sampler and tuned the sampler variance based on collision rate for the trade-off heuristically. Paxton et al. (2017) separates the action space into high-level discrete options and low-level continuous actions, and only considered the trade-off at the discrete option level, ignoring the exploration-exploitation in the fine action space. These existing works address the trade-off in an ad-hoc way, which may be inferior for the balance.

2 Settings for Learning to Plan

Let $\mathcal{S} \subseteq \mathbb{R}^q$ be the state space of the problem, *e.g.*, all the configurations of a robot and its base location in the workspace, $\mathcal{S}_{obs} \subsetneq \mathcal{S}$ be the obstacles set, $\mathcal{S}_{free} := \mathcal{S} \setminus \mathcal{S}_{obs}$ be the free space, $s_0 \in \mathcal{S}_{free}$ be the initial state and $\mathcal{S}_{goal} \subsetneq \mathcal{S}_{free}$ be the goal region. Then the space of all collision-free paths can be defined as a continuous function $\Xi := \{\xi(\cdot) : [0,1] \to \mathcal{S}_{free}\}$. Let $c(\cdot) : \Xi \mapsto \mathbb{R}$ be the cost functional over a path. The optimal path planning problem is to find the optimal path in terms of cost $c(\cdot)$ from start s_0 to goal $\mathcal{S}_{goal}$ in free space $\mathcal{S}_{free}$, *i.e.*,

$$\xi^* = \operatorname{argmin}_{\xi \in \Xi} c(\xi), \quad \text{s.t. } \xi(0) = s_0,\ \xi(1) \in \mathcal{S}_{goal}. \tag{1}$$

Traditionally (Karaman & Frazzoli, 2011), the planner has direct access to $(s_0, \mathcal{S}_{goal}, c(\cdot))$ and the workspace map (Ichter et al., 2018; Tamar et al., 2016; Lee et al., 2018), $\texttt{map}(\cdot) : \mathbb{R}^2$ or $\mathbb{R}^3 \mapsto \{0, 1\}$, (0: free spaces and 1: obstacles). Since $\mathcal{S}_{free}$ often has a very irregular geometry (illustrated in Figure 8 in Appendix A), it is usually represented via a *collision detection module* which is able to

detect the obstacles in a path segment. For the same reason, the feasible paths in Ξ are hard to be described in parametric forms, and thus, the nonparametric ξ, such as a sequence of interconnected path segments $[s_0, s_1], [s_1, s_2], \ldots, [s_{T-1}, s_T] \subset \mathcal{S}$ with $\xi(0) = s_0$ and $\xi(1) = s_T$, is used with an additive cost $\sum_{i=1}^{T} c([s_{i-1}, s_i])$.

Assuming given the planning problems $\{U_i := (s_0, \mathcal{S}_{goal}, \mathcal{S}, \mathcal{S}_{free}, \texttt{map}, c(\cdot))\}_{i=1}^{N}$ sampled from some distribution $\mathcal{U}$, we are interested in learning an algorithm $\texttt{alg}(\cdot)$, which can produce the (nearly)-optimal path efficiently from the observed planning problems. Formally, the *learning to plan* is defined as

$$\texttt{alg}^*(\cdot) = \text{argmin}_{\texttt{alg} \in \mathcal{A}} \, \mathbb{E}_{U \in \mathcal{U}} \left[\ell \left(\texttt{alg}(U) \right) \right], \tag{2}$$

where $\mathcal{A}$ denotes the planning algorithm family, and $\ell(\cdot)$ denotes some loss function which evaluates the quality of the generated path and the efficiency of the $\texttt{alg}(\cdot)$, *e.g.*, size of the search tree. We elaborate each component in Eq (2) in the following sections. We first introduce the tree-based sampling algorithm template in Section 3, upon which we instantiate the $\texttt{alg}(\cdot)$ via a novel attention-based neural parametrization in Section 4.2 with exploration-exploitation balance mechanism in Section 4.1. We design the ℓ-loss function and the meta learning algorithm in Section 4.3. Composing every component together, we obtain the neural exploration-exploitation trees (NEXT) which achieves outstanding performances in Section 5.

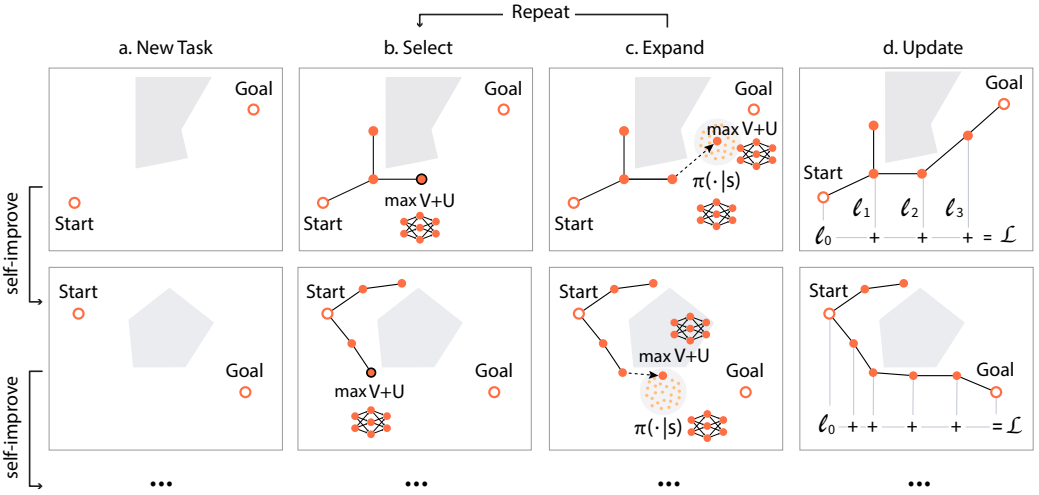

Figure 1: Illustration of NEXT. In each epoch, NEXT is executed on a randomly generated planning problem. The search tree grows with $\tilde{V}^*$ and $\tilde{\pi}^*$ guidance. $\{\tilde{V}^*, \tilde{\pi}^*\}$ will be updated according to the successful path. Such planning and learning iteration is continued interactively.

3 Preliminaries

The sampling-based planners are more practical and become dominant for high-dimensional path planning problems (Elbanhawi & Simic, 2014). We describe a unifying view for many existing tree-based sampling algorithms (TSA), which we will also base our algorithm upon. More specifically, this family of algorithms maintain a search tree $\mathcal{T}$ rooted at the initial point s_{init} and connecting all sampled points $\mathcal{V}$ in the configuration space with edge set $\mathcal{E}$. The tree will be expanded by incorporating more sampled states until some leaf reaches $\mathcal{S}_{goal}$. Then, a feasible solution for the path planning problem will be extracted based on the tree $\mathcal{T}$.

Algorithm 1: Tree-based Sampling Algorithm

Problem: $U = (s_{init}, \mathcal{S}_{goal}, \mathcal{S}, \mathcal{S}_{free}, \texttt{map}, c(\cdot))$;
Initialize $\mathcal{T} = (\mathcal{V}, \mathcal{E})$ with $\mathcal{V} \leftarrow \{s_{init}\}$, $\mathcal{E} \leftarrow \emptyset$;
for $t \leftarrow 0$ **to** T **do**
  $s_{parent}, s_{new} \leftarrow \texttt{Expand}(\mathcal{T}, U)$;
  if $\texttt{ObstacleFree}(s_{parent}, s_{new})$ **then**
    $\mathcal{V} \leftarrow \mathcal{V} \cup \{s_{new}\}$ and
     $\mathcal{E} \leftarrow \mathcal{E} \cup \{[s_{parent}, s_{new}]\}$;
    $\mathcal{T} \leftarrow \texttt{Postprocess}(\mathcal{T}, U)$;
     ▷ Optional
    if $s_{new} \in \mathcal{S}_{goal}$ **then**
      return $\mathcal{T}$;

The template of tree-based sampling algorithms is summarized in Algorithm 1 and illustrated in Fig. 1(c). A key component of the algorithm is the Expand operator, which generates the next exploration point s_{new} and its parent $s_{parent} \in \mathcal{V}$. To ensure the feasibility of the solution, the s_{new} must be **reachable** from $\mathcal{T}$, *i.e.*, $[s_{parent}, s_{new}]$ is collision-free, which is checked by a collision

detection function. As we will discuss in Appendix B, by instantiating different Expand operators, we will arrive at many existing algorithms, such as RRT (LaValle, 1998) and EST (Hsu et al., 1997; Phillips et al., 2004).

One major limitation of existing TSAs is that they solve each problem independently from scratch and ignore past planning experiences in similar environments. We introduce the neural components into TSA template to form the learnable planning algorithm family $\mathcal{A}$, which can explicitly take advantages of the past successful experiences to bias the Expand towards more promising regions.

4 Neural Exploration-Exploitation Trees

Based on the TSA framework, we introduce a *learnable neural based* Expand operator, which can balance between exploration and exploitation, to instantiate $\mathcal{A}$ in Eq (2). With the self-improving training, we obtain the meta NEXT algorithm illustrated in Figure 1.

4.1 Guided Progressive Expansion

We start with our design of the Expand. We assume having an estimated value function $\tilde{V}^*(s|U)$, which stands for the optimal cost from s to target in planning problem U, and a policy $\tilde{\pi}^*(s'|s,U)$, which generates the promising action s' from state s. The concrete parametrization of $\tilde{V}^*$ and $\tilde{\pi}^*$ will be explained in Section 4.2 and learned in Section 4.3. We will use these functions to construct the learnable Expand with explicit exploration-exploitation balancing.

Algorithm 2: NEXT :: Expand$(\mathcal{T}=(\mathcal{V},\mathcal{E}),U)$

1 $s_{parent} \leftarrow \text{argmax}_{s\in\mathcal{V}}\, \phi(s)$; ▷ Selection
2 $\{s_1,\dots,s_k\} \overset{iid.}{\sim} \tilde{\pi}^*(s'|s_{parent},U)$; ▷ Candidates
3 $s_{new} \leftarrow \text{argmax}_{s'\in\{s_1,\dots,s_k\}}\, \phi(s')$; ▷ Expansion
4 **return** s_{parent}, s_{new};

The Expand operator will expand the current search tree $\mathcal{T}$ by a new neighboring state s_{new} around $\mathcal{T}$. We design the expansion as a two-step procedure: **(i)** select a state s_{parent} from existing tree $\mathcal{T}$; **(ii)** expand a state s_{new} in the neighborhood of s_{parent}. More specifically,

Selecting s_{parent} from $\mathcal{T}$ in step (i). Consider the negative value function $-\tilde{V}^*(s|U)$ as the rewards $r(s)$, step **(i)** shares some similarity with the multi-armed bandit problem by viewing existing nodes $s\in\mathcal{V}$ as arms. However, the vanilla UCB algorithm is not directly applicable, since the number of states is increasing as the algorithm proceeds and the value of these adjacent states are naturally correlated. We address this challenge by modeling the correlation explicitly as in contextual bandits. Specifically, we parametrize the UCB of the reward function as $\phi(s)$, and select a node from $\mathcal{T}$ according to $\phi(s)$

$$s_{parent} = \text{argmax}_{s\in\mathcal{V}} \quad \phi(s) := \bar{r}_t(s) + \lambda\sigma_t(s), \tag{3}$$

where $\bar{r}_t$ and σ_t denote the average reward and variance estimator after t-calls to Expand. Denote the sequence of t selected tree nodes so far as $\mathcal{S}_t = \{s^1_{parent},\dots,s^t_{parent}\}$, then we can use kernel smoothing estimator for $\bar{r}_t(s) = \frac{\sum_{s'\in\mathcal{S}_t} k(s',s)r(s')}{\sum_{s'\in\mathcal{S}_t} k(s',s)}$ and $\sigma_t(s) = \sqrt{\frac{\log\sum_{s'\in\mathcal{S}_t} w(s')}{w(s)}}$ where $k(s',s)$ is a kernel function and $w(s) = \sum_{s'\in\mathcal{S}_t} k(s',s)$. Other parametrizations of $\bar{r}_t$ and σ_t are also possible, such as Gaussian Process parametrization in Appendix C. The average reward exploits more promising states, while the variance promotes exploration towards less frequently visited states; and the exploration versus exploitation is balanced by a tunable weight $\lambda > 0$.

Expanding a reachable s_{new} in step (ii). Given the selected s_{parent}, we consider expanding a reachable state in the neighborhood s_{parent} as an *infinite-armed* bandit problem. Although one can first samples k arms uniformly from a neighborhood around s_{parent} and runs a UCB algorithm on the randomly generated finite arms (Wang et al., 2009), such uniform sampler ignores problem structures, and will lead to unnecessary samples. Instead we will employ a policy $\tilde{\pi}^*(s'|s,U)$[1] for guidance when generating the candidates. The final choice for next move will be selected from these candidates with $\max\phi(s)$ defined in (3). As explained in more details in Section 4.2, $\tilde{\pi}^*$ will be trained to mimic previous successful planning experiences across different problems, that is, biasing the sampling towards the states with higher successful probability.

With these detailed step **(i)** and **(ii)**, we obtain NEXT :: Expand in Algorithm 2 (illustrated in Figure 1(b) and (c)). Plugging it into the TSA in 1, we construct $\texttt{alg}(\cdot) \in \mathcal{A}$ which will be learned.

[1] In the path planning setting, we use $\tilde{\pi}^*(s'|s,U)$ and $\tilde{\pi}^*(a|s,U)$ interchangeably as the action is next state.

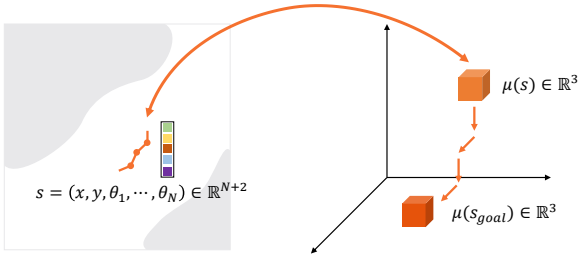

Figure 2: Our neural network model maps a N-link robot from the original planning space (a $(N+2)$-d configuration space) to a 3d discrete latent planning space in which we plan a path using value iteration. The result of value iteration is then used as features for defining $\tilde{V}^*(s|U)$ and $\tilde{\pi}^*(s'|s, U)$.

The guided progressive expansion bears similarity to MCTS but deals with high dimensional continuous spaces. Moreover, the essential difference lies in the way to select state in $\mathcal{T}$ for expansion: the MCTS only expands the leaf states in $\mathcal{T}$ due to the hierarchical assumption, limiting the exploration ability and incurring extra unnecessary UCB sampling for internal traversal in $\mathcal{T}$; while the proposed operation enables expansion from each visited state, particularly suitable for path planning problems.

4.2 Neural Architecture for Value Function and Expansion Policy

In this section, we will introduce our neural architectures for $\tilde{V}^*(s|U)$ and $\tilde{\pi}^*(s'|s, U)$ used in `NEXT :: Expand`. The proposed neural architectures can be understood as first embedding the state and problem into a **discrete** latent representation, upon which neuralized value iteration is performed to extract features for defining $\tilde{V}^*(s|U)$ and $\tilde{\pi}^*(s'|s, U)$, as illustrated in Figure 2.

Configuration space embedding. Our network for embedding high-dimension configuration space into a latent representation is designed based on an attention mechanism. More specifically, let s^w denote the workspace in state and s^h denote the remaining dimensions of the state, *i.e.* $s = (s^w, s^h)$. s^w and s^h will be embedded by different sub-neural networks and combined for the final representation, as illustrated in Figure 3. For simplicity of exposition, we will focus on the 2d workspace, *i.e.*, $s^w \in \mathbb{R}^2$. However, our method applies to 3d workspace as well.

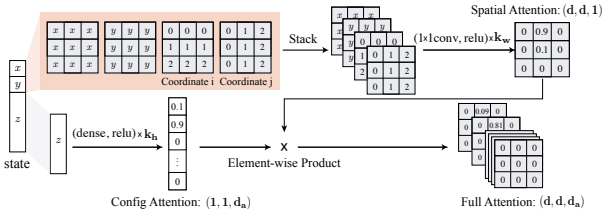

Figure 3: Attention-based state embedding module. $s^w = (x, y)$ and $\mathbf{z} = s^h$. The upper part is spatial attention, with the first two channels being x and y, and the last two channels being constant templates with the row and column coordinates, as shown with a d set to 3. The bottom module learns the representation for $\mathbf{z}$. The final embedding is obtained by outer-product of these two attention parts.

- **Spatial attention.** The workspace information s^w will be embedded as $\mu^w(s^w) \in \mathbb{R}^{d \times d}$, d is a hyperparameter related to `map` (see remark below). The spatial embedding module is composed of k_w convolution layers, *i.e.*,
$$\mu^w(s^w) = \texttt{softmax2d}(f^w_{k_w}(s^w)), \qquad f^w_{i+1}(s^w) = \texttt{relu}(\theta^w_i \oplus f^w_i(s^w)), \tag{4}$$
where θ^w_i denotes the convolution kernels, $\oplus$ denotes the convolution operator and $f^w_i(s^w) \in \mathbb{R}^{d \times d \times d_i}$ with d_i channels. The first layer f^w_0 is designed to represent s^w into a $d \times d \times 4$ tensor as $f^w_0(s^w)_{ij} = [s^w_1, s^w_2, i, j]$, $i, j = 1, \ldots, d$, without any loss of information.
- **Configuration attention.** The remaining configuration state information will be embedded as $\mu^h(s^h)$ through k_h fully-connected layers, *i.e.*
$$\mu^h(s^h) = \texttt{softmax}(f^h_{k_h}(s^h)), \qquad f^h_{i+1}(s^h) = \texttt{relu}(\theta^h_i f^h_i(s^h) + b_i),$$
where $\mu^h(s^h) \in \mathbb{R}^{d_a}$ and $f^h_0(s^h) = s^h$.

The final representation $\mu_\theta(s)$ will be obtained by multiplying $\mu^w(s^w)$ with $\mu^h(s^h)$ element-wisely, $\mu_\theta(s)_{ijl} = \mu^w(s^w)_{ij} \cdot \mu^h(s^h)_l$, which is a $d \times d \times d_a$ tensor attention map with $\mu_\theta(s)_{ijl} \geqslant 0$, and $\sum_{ijl} \mu_\theta(s)_{ijl} = 1$. Intuitively, one can think of d_a as the level of the *learned discretization* of the configuration space s^h, and the entries in μ softly assign the actual state s to these discretized locations. $\theta := (\{\theta^w_i\}_{i=0}^{k_w - 1}, \{\theta^h_i, b_i\}_{i=0}^{k_h - 1})$ are the set of parameters to learn.

Remark (different map size): To process `map` using convolution neural networks, we resize it to a $d \times d$ image, with the same size as the spatial attention in Eq (4), where d is a hyperparameter.

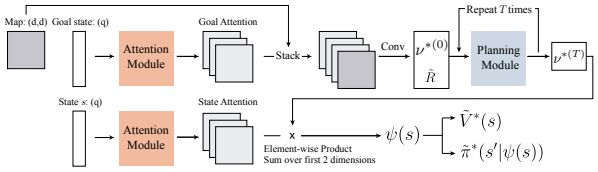

Figure 4: Overall model architecture. Current and goal states are embedded through attention module. Then the embedding of the goal state is concatenated with the map to produce $\nu^{*(0)}$ and $\tilde{R}$ as the input to the planning module. The output of the planning module is aggregated with the embedding of the current state to produce feature $\psi(s)$ for defining $\tilde{V}^*$ and $\tilde{\pi}^*$.

Neural value iteration. We will apply neuralized value iteration on top of the configuration space embedding to extract further features (Tamar et al., 2016; Lee et al., 2018). First, we produce the embedding $\mu_\theta(s_{goal})$ of the center of the goal region s_{goal}. Then we execute T steps of neuralized Bellman updates in the embedding space,

$$\nu^{*(t)} = \min\left(W_1 \oplus \left[\nu^{*(t-1)}, \tilde{R}\right]\right), \quad \text{with} \quad (\nu^{*(0)}, \tilde{R}) = \sigma\left(W_0 \oplus [\mu_\theta(s_{goal}), \texttt{map}]\right),$$

and obtain $\nu^{*(T)} \in \mathbb{R}^{d\times d\times d_a\times p}$. Both W_0 and W_1 are 3d convolution kernels, $\min$ implements the pooling across channels. Accordingly, $\nu^{*(T)}$ now can be understood as a latent representation of the value function $\tilde{V}^*(\cdot)$ in learned embedding space for the problem U with s_{goal} in $\texttt{map}$.

To define the value function for particular state s, *i.e.*, $\tilde{V}^*(s|U)$, from the latent representation $\nu^{*(T)}$, we first construct another attention model between the embedding of state s using $\mu_\theta(s)$ and $\nu^{*(T)}$, *i.e.*, $\psi(s)_k = \sum_{ijl} \nu^{*(T)}_{ijlk} \cdot \mu_\theta(s)_{ijl}$, for $k = 1, \ldots, p$. Finally we define

$$\tilde{V}^*(s|U) = h_{W_2}(\psi(s)), \quad \text{and} \quad \tilde{\pi}^*(s'|s,U) = \mathcal{N}(h_{W_3}(\psi(s)), \sigma^2) \tag{5}$$

where h_{W_2} and h_{W_3} are fully connected dense layers with parameters W_2 and W_3 respectively, and $\mathcal{N}(h_{W_3}(\psi(s)), \sigma^2)$ is a Gaussian distribution with variance σ^2. Note that we also parametrize the policy $\tilde{\pi}^*(s'|s,U)$ using the embedding $\nu^{*(T)}$, since the policy is connected to the value function via $\pi^*(s'|s,U) = \text{argmin}_{s'\in\mathcal{S}}\, c([s,s']) + V^*(s'|U)$. It should also be emphasized that in our parametrization, the calculation of $\nu^{*(T)}$ only relies on the $\mu_\theta(s_{goal})$, which can be reused for evaluating $\tilde{V}^*(s|U)$ and $\tilde{\pi}^*(s'|s,U)$ over different s, saving computational resources.

The overall model architecture in $\texttt{alg}(\cdot)$ is illustrated in Figure 4. The parameters $W = (W_0, W_1, W_2, W_3, \theta)$ will be learned together by our *meta self-improving learning*. For the details of the parameterization and the size of convolution kernels in our implementation, please refer to Figure 10 in Appendix D.

4.3 META SELF-IMPROVING LEARNING

The learning of the planner $\texttt{alg}(\cdot)$ reduces to learning the parameters in $\tilde{V}^*(s|U)$ and $\tilde{\pi}^*(s'|s,U)$ and is carried out while planning experiences accumulate. We do not have an explicit training and testing phase separation. Particularly, we use a mixture of $\texttt{RRT}::\texttt{Expand}$ and $\texttt{NEXT}::\texttt{Expand}$ with probability ϵ and $1-\epsilon$, respectively, inside the $\texttt{TSA}$ framework in Algorithm 1. The RRT* postprocessing step is used in the template. The ϵ is set to be 1 initially since $\{\tilde{V}^*, \tilde{\pi}^*\}$ are not well-trained, and thus, the algorithm behaves like RRT*. As the training proceeds, we anneal ϵ gradually as the sampler becomes more efficient.

Algorithm 3: Meta Self-Improving Learning

```
Initialize dataset D_0;
for epoch n ← 1 to N do
    Sample a planning problem U;
    T ← TSA(U) with ε ~ Unif[0,1], and
      ε · RRT :: Expand + (1 − ε) · NEXT :: Expand;
      Postprocessing with RRT* :: Postprocess;
    D_n ← D_{n−1} ∪ {(T, U)} if successful else
      D_{n−1};
    for j ← 0 to L do
        Sample (T_j, U_j) from D_n;
        Reconstruct optimal path {s^i}_{i=1}^m and the
          cost of paths based on T_j;
        Update parameters
          W ← W − η∇_W ℓ(Ṽ*, π̃*; T_j, U_j);
    Anneal ε = αε, α ∈ (0,1);
```

The dataset $\mathcal{D}_n = \{(\mathcal{T}_j, U_j)\}_{j=1}^n$ for the n-th training epoch is collected from the previous successful planning experiences across *multiple random problems*. We fix the size of dataset and update $\mathcal{D}$ in the same way as experience reply buffer (Lin, 1992; Schaul et al., 2015). For an experience $(\mathcal{T}, U) \in \mathcal{D}_n$, we can reconstruct the successful path $\{s^i\}_{i=1}^m$ from the search tree $\mathcal{T}$ (m is the number of segments), and the value of each state s^i in the path will be the sum of cost to the

goal region, *i.e.*, $y^i := \sum_{l=i}^{m-1} c([s^l, s^{l+1}])$. We learn $\{\tilde{V}^*, \tilde{\pi}^*\}$ by optimizing objective

$$\min_{W} \sum_{(\mathcal{T},U)\in\mathcal{D}_n} \ell(\tilde{V}^*, \tilde{\pi}^*; \mathcal{T}, U) := -\sum_{\mathcal{D}_n} \sum_{i=1}^{m-1} \log \tilde{\pi}^* \left(s^{i+1}|s^i\right) + \sum_{i=1}^{m} (\tilde{V}^* \left(s^i\right) - y^i)_2^2 + \lambda \left\|W\right\|^2. \quad (6)$$

The loss (6) pushes the $\tilde{V}^*$ and $\tilde{\pi}^*$ to chase the successful trajectories, providing effective guidance in $\texttt{alg}(\cdot)$ for searching, and therefore leading to efficient searching procedure with less sample complexity and better solution. On one hand, the value function and policy estimation $\{\tilde{V}^*, \tilde{\pi}^*\}$ is improved based upon the successful outcomes from NEXT itself on previous problems. On the other hand, the updated $\{\tilde{V}^*, \tilde{\pi}^*\}$ will be applied in the next epoch to improve the performance. Therefore, the training is named as *Meta Self-Improving Learning (MSIL)*. Since all the trajectories we collected for learning are feasible, the reachability of the proposed samples is enforced implicitly via imitating these successful paths.

By putting every components together into the learning to plan framework in Eq (2), the overall procedure is summarized in Algorithm 3 and illustrated in Figure 1.

5 EXPERIMENTS

In this section, we evaluate the proposed NEXT empirically on different planning tasks in a variety of environments. Comparing to the existing planning algorithms, NEXT achieves the state-of-the-art performances, in terms of both success rate and the quality of the found solutions. We further demonstrate the power of the proposed two components by the corresponding ablation study.

Benchmark environments. We designed four benchmark tasks to demonstrate the effectiveness of our algorithm for high-dimensional planning. The first three involve planning in a 2d workspace with a 2 DoF (degrees of freedom) point robot, a 3 DoF stick robot and a 5 DoF snake robot, respectively. The last one involves planning a 7 DoF spacecraft in a 3d workspace. For all problems in each benchmark task, the workspace maps were randomly generated from a fixed distribution; the initial and goal states were sampled uniformly randomly in the free space; the cost function $c(\cdot)$ was set as the sum of the Euclidean path length and the control effort penalty of rotating the robot joints.

Baselines. We compared NEXT with RRT* (Karaman & Frazzoli, 2011), BIT* (Gammell et al., 2015), CVAE-plan (Ichter et al., 2018), Reinforce-plan (Zhang et al., 2018), and an improved version of GPPN (Lee et al., 2018) in terms of both planning time and solution quality. RRT* and BIT* are two widely used effective instances of `TSA` in Algorithm 1. In our experiments, we equipped RRT* with the goal biasing heuristic to improve its performance. BIT* adopts the informed search strategy (Gammell et al., 2015) to accelerate planning. CVAE-plan and Reinforce-plan are two learning-enhanced `TSA` planners proposed recently. CVAE-plan learns a conditional VAE as the sampler (Sohn et al., 2015), which will be trained by near-optimal paths produced by RRT*. Reinforce-plan learns to do rejection sampling with policy gradient methods. For the improved GPPN, we combined its architecture for `map` with a fully-connected MLP for the rest state, such that it can be applied to high-dimensional continuous spaces. Please refer to Appendix E for more details.

Settings. For each task, we randomly generated 3000 different problems from the same distribution without duplicated maps. We trained all learning-based baselines using the first 2000 problems, and reserved the rest for testing. The parameters for RRT* and BIT* are also tuned using the first 2000 problems. For NEXT, we let it improve itself using MSIL over the first 2000 problems. In this period, for every 200 problems, we updated its parameters and annealed ϵ once.

Comparison results. Examples of all four environments are illustrated in Appendix F.1 and Figure 6, where NEXT finds high-quality solutions as shown. We also illustrated the comparison of the search trees on two 2d and 7d planning tasks between NEXT and RRT* in Figure 5 (a)-(c) and Figure 6 (b)-(c). Obviously, the proposed NEXT algorithm explores with guidance and achieves better quality solutions with fewer samples, while the RRT* expands randomly which may fail to find a solution. The learned $\tilde{V}^*$ and $\tilde{\pi}^*$ in the 2d task are also shown in Figure 5(d). As we can see, they are consistent with our expectation, towards the ultimate target in the map. For more search tree comparisons for all four experiments, please check Figure 16, 17, 18 and 19 in Appendix F.

To systematically evaluate the algorithms, we recorded the cost of time (measured by the number of collision checks used) to find a collision-free path, the success rate within time limits, and the cost of the solution path for each run. The results of the reserved 1000 test problems of each environment are

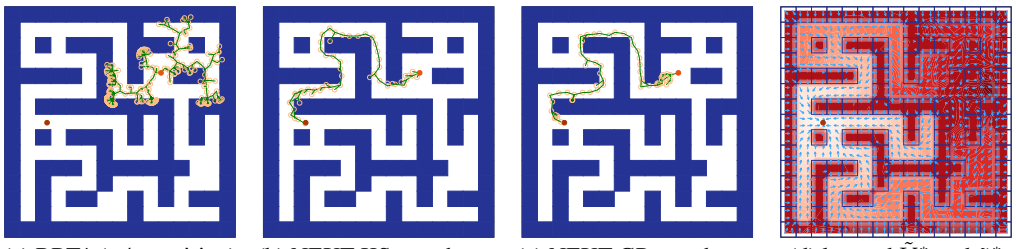

(a) RRT* (w/o rewiring) (b) NEXT-KS search tree (c) NEXT-GP search tree (d) learned $\tilde{V}^*$ and $\tilde{\pi}^*$

Figure 5: Search trees and the learned $\tilde{V}^*$ and $\tilde{\pi}^*$ produced by NEXT. Obstacles are colored in blue. The start and goal locations are denoted by orange and brown dots. In (a) to (c), samples are represented with yellow circles. In (d), the level of redness denotes the value of the cost-to-go estimate $\tilde{V}^*$. The cyan arrows point from a given state s to the mean of the learned policy $\tilde{\pi}^*(s'|s, U)$.

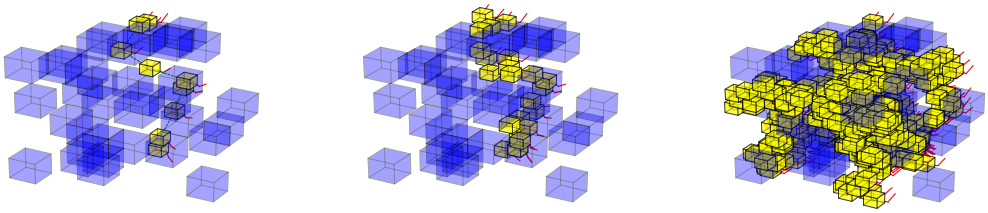

(a) NEXT-KS solution path (b) NEXT-KS search tree (c) RRT* search tree (w/o rewiring)

Figure 6: Search trees and a solution path produced in an instance of spacecraft planning. The 7 DOF spacecraft has a yellow body and two 2 DOF red arms. NEXT-KS produced a nearly minimum viable search tree while RRT* failed to find a path within limited trials.

shown in the top row of Figure 7. We set the maximal number of samples as 500 for all algorithms. Both the kernel smoothing (NEXT-KS) and the Gaussian process (NEXT-GP) version of NEXT achieves the state-of-the-art performances, under all three criteria in all test environments. Although the BIT* utilizes the heuristic particularly suitable for 3d maze in 7d task and performs quite well, the NEXT algorithm still outperform every competitor by a large margin, no matter learning-based or prefixed heuristic planner, demonstrating the advantages of the proposed NEXT algorithm.

Ablation study I: guided progressive expansion. To demonstrate the power of `NEXT :: Expand`, we replace it with breadth-first search (BFS) (Kim et al., 2018), another expanding strategy, while keeping other components the same. Specifically, BFS uses a search queue in planning. It repeatedly pops a state s out from the search queue, samples k states from $\pi(\cdot|s)$, and pushes all generated samples and state s back to the queue, until the goal is reached. For fairness, we use the learned sampling policy $\pi(s'|s, U)$ by NEXT-KS in BFS. As shown in Figure 7, BFS obtained worse paths with a much larger number of collision checks and far lower success rate, which justifies the importance of the balance between exploration versus exploitation achieved by the proposed `NEXT :: Expand`.

Ablation study II: neural architecture. To further demonstrate the benefits of the proposed neural architecture for learning generalizable representations in high-dimension planning problems, We replaced our attention-based neural architecture with an improved GPPN, as explained in Appendix E, for ablation study. We extended the GPPN for continuous space by adding an extra reactive policy network to its final layers. We emphasize the original GPPN is not applicable to the tasks in our experiments. Intuitively, the improved GPPN first produces a 'rough plan' by processing the robot's discretized workspace positions. Then the reactive policy network predicts a continuous action from both the workspace feature and the full configuration state of the robot. We provide more preference to the improved GPPN by training it to imitate the near-optimal paths produced by RRT* in the training problems. During test time it is also combined with both versions of the guided progressive expansion operators. As we can see, both GPPN-KS and GPPN-GP are clearly much worse than NEXT-KS and NEXT-GP, demonstrating the advantage of our proposed attention-based neural architecture in high-dimensional planning tasks.

Ablation study III: learning versus heuristic. The NEXT algorithm in Figure 5 shows similar behavior as the Dijkstra heuristic, *i.e.* sampling on the shortest path connecting the start and the goal in workspace. However, in higher dimensional space, the Dijkstra heuristic will fail. To demonstrate that, we replace the policy and value network with Dijkstra heuristic, using the best direction in

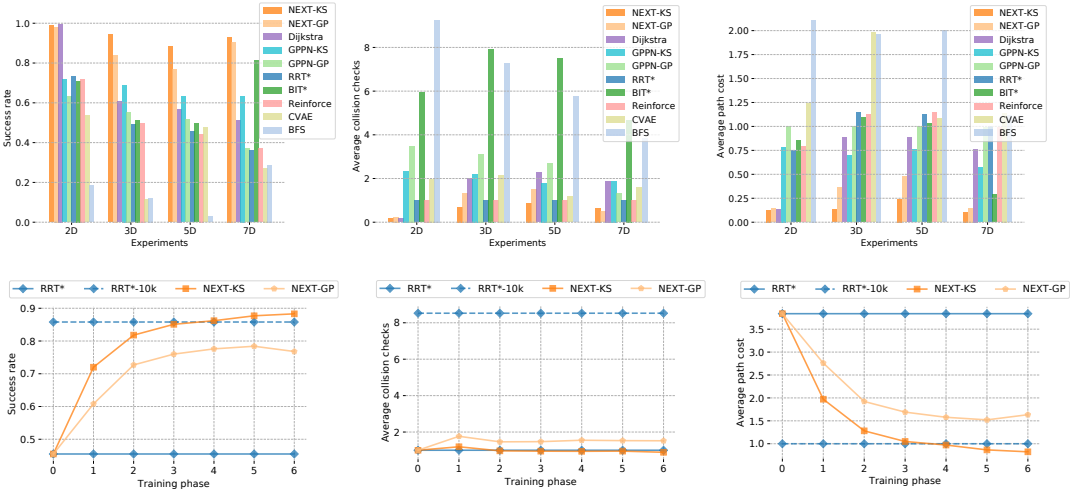

Figure 7: First row: histograms of results, in terms of success rate, average collision checks, and average cost of the solution paths; Second row: NEXT improvement curves in the 5d experiments. All algorithms are set to use up to 500 samples, except RRT*-10k, which uses 10,000 samples. The value of collision checks and path costs are normalized w.r.t. the performance of RRT*.

workspace to guide sampling. NEXT performs much better than Dijkstra in all but the 2d case, in which the workspace happens to be the state space.

Self-improving. We plot the performance improvement curves of our algorithms on the 5d planning task in the bottom row of Figure 7. For comparison, we also plot the performance of RRT*. At the beginning phase of self-improving, our algorithms are comparable to RRT*. They then gradually learn from previous experiences and improve themselves as they see more problems and better solutions. In the end, NEXT-KS is able to match the performance of RRT*-10k using only one-twentieth of its samples, while the competitors perform consistently without any improvements.

Due to the space limits, we put improvement curves on other environments in Figure 15 and the quantitative evaluation in Table 1, 2, and 3 in Appendix F. Please refer to the details there.

6 Conclusion

In this paper, we propose a self-improving planner, Neural EXploration-EXploitation Trees (NEXT), which can generalize and achieve better performance with experiences accumulated. The algorithm achieves a delicate balance between exploration-exploitation via our carefully designed UCB-type expansion operation. To obtain the generalizable ability across different problems, we proposed a new parametrization for the value function and policy, which captures the Bellman recursive structure in the high-dimensional continuous state and action space. We demonstrate the power of the proposed algorithm by outperforming previous state-of-the-art planners with significant margins on planning problems in a variety of different environments.

References

Auer, P., Cesa-Bianchi, N., and Fischer, P. Finite-time analysis of the multiarmed bandit problem. *Machine learning*, 47(2-3):235–256, 2002.

Mohak Bhardwaj, Sanjiban Choudhury, and Sebastian Scherer. Learning heuristic search via imitation. *arXiv preprint arXiv:1707.03034*, 2017.

Boor, V., Overmars, M. H., and Van Der Stappen, A. F. The gaussian sampling strategy for probabilistic roadmap planners. In *Robotics and automation, 1999. proceedings. 1999 ieee international conference on*, volume 2, pp. 1018–1023. IEEE, 1999.

Burns, B. and Brock, O. Sampling-based motion planning using predictive models. In *Robotics and Automation, 2005. ICRA 2005. Proceedings of the 2005 IEEE International Conference on*, pp. 3120–3125. IEEE, 2005a.

Burns, B. and Brock, O. Toward optimal configuration space sampling. In *Robotics: Science and Systems*, pp. 105–112. Citeseer, 2005b.

Bowen, Chris, and Ron Alterovitz. Closed-loop global motion planning for reactive execution of learned tasks. In *IEEE/RSJ International Conference on Intelligent Robots and Systems*, pp. 1754-1760, 2014.

Cadena Cesar, Luca Carlone, Henry Carrillo, Yasir Latif, Davide Scaramuzza, José Neira, Ian Reid, and John J. Leonard. Past, present, and future of simultaneous localization and mapping: Toward the robust-perception age. *IEEE Transactions on Robotics*, 32(6), 2016.

Chu, W., Li, L., Reyzin, L., and Schapire, R. Contextual bandits with linear payoff functions. In *Proceedings of the Fourteenth International Conference on Artificial Intelligence and Statistics*, pp. 208–214, 2011.

Couëtoux, A., Hoock, J.-B., Sokolovska, N., Teytaud, O., and Bonnard, N. Continuous upper confidence trees. In *International Conference on Learning and Intelligent Optimization*, pp. 433–445. Springer, 2011.

Silver, David and Hubert, Thomas and Schrittwieser, Julian and Antonoglou, Ioannis and Lai, Matthew and Guez, Arthur and Lanctot, Marc and Sifre, Laurent and Kumaran, Dharshan and Graepel, Thore and others Mastering chess and shogi by self-play with a general reinforcement learning algorithm. *arXiv preprint arXiv:1712.01815*, 2017.

Rosen Diankov and James Kuffner. Randomized statistical path planning. In *2007 IEEE/RSJ International Conference on Intelligent Robots and Systems*, pp. 1–6. IEEE, 2007.

Elbanhawi, M. and Simic, M. Sampling-based robot motion planning: A review. *Ieee access*, 2: 56–77, 2014.

Finney, S., Kaelbling, L. P., and Lozano-Perez, T. Predicting partial paths from planning problem parameters. In *Robotics Science and Systems*, 2007.

Fulgenzi, Chiara and Tay, Christopher and Spalanzani, Anne and Laugier, Christian Probabilistic navigation in dynamic environment using rapidly-exploring random trees and gaussian processes In *IEEE/RSJ International Conference on Intelligent Robots and Systems*, pp. 1056–1062, 2008.

Gammell, J. D., Srinivasa, S. S., and Barfoot, T. D. Informed rrt*: Optimal sampling-based path planning focused via direct sampling of an admissible ellipsoidal heuristic. *arXiv preprint arXiv:1404.2334*, 2014.

Gammell, J. D., Srinivasa, S. S., and Barfoot, T. D. Batch informed trees (bit*): Sampling-based optimal planning via the heuristically guided search of implicit random geometric graphs. In *Robotics and Automation (ICRA), 2015 IEEE International Conference on*, pp. 3067–3074. IEEE, 2015.

Guez, Arthur and Weber, Théophane and Antonoglou, Ioannis and Simonyan, Karen and Vinyals, Oriol and Wierstra, Daan and Munos, Rémi and Silver, David Learning to search with mctsnets *arXiv preprint arXiv:1802.04697*, 2018.

Peter E Hart, Nils J Nilsson, and Bertram Raphael. A formal basis for the heuristic determination of minimum cost paths. *IEEE transactions on Systems Science and Cybernetics*, 4(2):100–107, 1968.

Hsu, D., Latombe, J.-C., and Motwani, R. Path planning in expansive configuration spaces. In *Robotics and Automation, 1997. Proceedings., 1997 IEEE International Conference on*, volume 3, pp. 2719–2726. IEEE, 1997.

Hsu, D., Jiang, T., Reif, J., and Sun, Z. The bridge test for sampling narrow passages with probabilistic roadmap planners. In *Robotics and Automation, 2003. Proceedings. ICRA'03. IEEE International Conference on*, volume 3, pp. 4420–4426. IEEE, 2003.

Hsu, D., Sánchez-Ante, G., and Sun, Z. Hybrid prm sampling with a cost-sensitive adaptive strategy. In *Robotics and Automation, 2005. ICRA 2005. Proceedings of the 2005 IEEE International Conference on*, pp. 3874–3880. IEEE, 2005.

Huh, Jinwook and Lee, Daniel Efficient Sampling With Q-Learning to Guide Rapidly Exploring Random Trees. *IEEE Robotics and Automation Letters*, 3:3868–3875, 2018.

Ichter, B., Harrison, J., and Pavone, M. Learning sampling distributions for robot motion planning. In *2018 IEEE International Conference on Robotics and Automation (ICRA)*, pp. 7087–7094. IEEE, 2018.

Karaman, S. and Frazzoli, E. Sampling-based algorithms for optimal motion planning. *The international journal of robotics research*, 30(7):846–894, 2011.

Karkus, P., Hsu, D., and Lee, W. S. Qmdp-net: Deep learning for planning under partial observability. In *Advances in Neural Information Processing Systems*, pp. 4694–4704, 2017.

Kavraki, L. E., Svestka, P., Latombe, J.-C., and Overmars, M. H. Probabilistic roadmaps for path planning in high-dimensional configuration spaces. *IEEE Transactions on Robotics and Automation*, 12(4), 1996.

Kim, B., Kaelbling, L. P., and Lozano-Pérez, T. Guiding search in continuous state-action spaces by learning an action sampler from off-target search experience. 2018.

Kocsis, L. and Szepesvári, C. Bandit based monte-carlo planning. In *European conference on machine learning*, pp. 282–293. Springer, 2006.

Krause, A. and Ong, C. S. Contextual gaussian process bandit optimization. In *Advances in Neural Information Processing Systems*, pp. 2447–2455, 2011.

Kuo, Yen-Ling and Barbu, Andrei and Katz, Boris Deep sequential models for sampling-based planning In *IEEE/RSJ International Conference on Intelligent Robots and Systems*, pp. 6490–6497, 2018.

Langford, J. and Zhang, T. The epoch-greedy algorithm for multi-armed bandits with side information. In *Advances in neural information processing systems*, pp. 817–824, 2008.

LaValle, S. M. Rapidly-exploring random trees: A new tool for path planning. 1998.

Lee, L., Parisotto, E., Chaplot, D. S., Xing, E., and Salakhutdinov, R. Gated path planning networks. *arXiv preprint arXiv:1806.06408*, 2018.

Long-Ji Lin. Self-improving reactive agents based on reinforcement learning, planning and teaching. *Machine learning*, 8(3-4):293–321, 1992.

Paxton, Chris and Raman, Vasumathi and Hager, Gregory D and Kobilarov, Marin Combining neural networks and tree search for task and motion planning in challenging environments In *IEEE/RSJ International Conference on Intelligent Robots and Systems (IROS)*, pp. 6059–6066, 2017.

Sven Mikael Persson and Inna Sharf. Sampling-based a* algorithm for robot path-planning. *The International Journal of Robotics Research*, 33(13):1683–1708, 2014.

Phillips, J. M., Bedrossian, N., and Kavraki, L. E. Guided expansive spaces trees: A search strategy for motion-and cost-constrained state spaces. In *IEEE International Conference on Robotics and Automation*, pp. 3968–3973, 2004.

Qureshi, Ahmed H and Simeonov, Anthony and Bency, Mayur J and Yip, Michael C. Motion planning networks. In *IEEE International Conference on Robotics and Automation*, 2019.

Reif, J. H. Complexity of the mover's problem and generalizations. In *Foundations of Computer Science, 1979., 20th Annual Symposium on*, pp. 421–427. IEEE, 1979.

Rickert, Markus and Brock, Oliver and Knoll, Alois. Balancing exploration and exploitation in motion planning In *IEEE International Conference on Robotics and Automation*, pp. 2812–2817. IEEE, 2008.

Tom Schaul, John Quan, Ioannis Antonoglou, and David Silver. Prioritized experience replay. *arXiv preprint arXiv:1511.05952*, 2015.

Shkolnik, A., Walter, M., and Tedrake, R. Reachability-guided sampling for planning under differential constraints. In *Robotics and Automation, 2009. ICRA'09. IEEE International Conference on*, pp. 2859–2865. IEEE, 2009.

Sohn, K., Lee, H., and Yan, X. Learning structured output representation using deep conditional generative models. In *Advances in Neural Information Processing Systems*, pp. 3483–3491, 2015.

Srinivas, N., Krause, A., Kakade, S. M., and Seeger, M. Gaussian process optimization in the bandit setting: No regret and experimental design. *arXiv preprint arXiv:0912.3995*, 2009.

Tamar, A., Wu, Y., Thomas, G., Levine, S., and Abbeel, P. Value iteration networks. In *Advances in Neural Information Processing Systems*, pp. 2154–2162, 2016.

Wang, Y., Audibert, J.-Y., and Munos, R. Algorithms for infinitely many-armed bandits. In *Advances in Neural Information Processing Systems*, pp. 1729–1736, 2009.

Ye, Gu and Alterovitz, Ron Guided motion planning. In *Robotics research*, pp. 291–6307. Springer, 2017.

Yee, T., Lisy, V., and Bowling, M. Monte carlo tree search in continuous action spaces with execution uncertainty. In *Proceedings of the Twenty-Fifth International Joint Conference on Artificial Intelligence*, pp. 690–696. AAAI Press, 2016.

Zhang, C., Huh, J., and Lee, D. D. Learning implicit sampling distributions for motion planning. *arXiv preprint arXiv:1806.01968*, 2018.

Zucker, M., Kuffner, J., and Bagnell, J. A. Adaptive workspace biasing for sampling-based planners. In *Robotics and Automation, 2008. ICRA 2008. IEEE International Conference on*, pp. 3757–3762. IEEE, 2008.

Appendix

A Illustration of the Difficulty in Planning Problems

The Figure 8(a) illustrates a concrete planning problem for a stick robot in 2d workspace. With one extra continuous action for rotation, the configuration state is visualized in Figure 8(b), which is highly irregular and unknown to the planner.

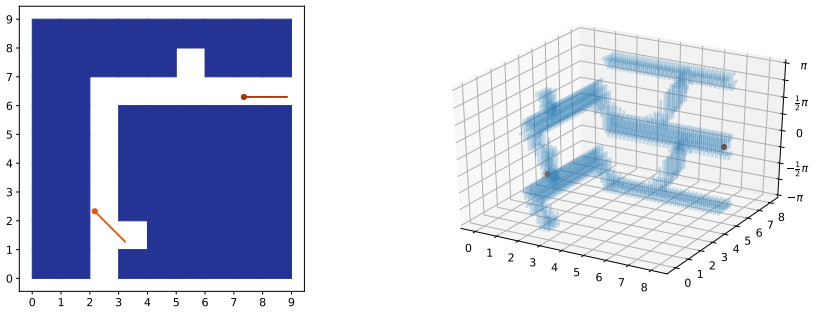

(a) Workspace (b) Configuration space

Figure 8: Different views of the same planning problem. In (a) we color the obstacles, the starting and the goal position of the robot in deep blue, orange and brown, respectively. The stick robot can move and rotate. The corresponding configuration space is 3d, as visualized in (b), with the extra dimension being the rotation angle w.r.t. the x-axis. The blue region indicates the feasible state space, *i.e.*, the set of collision-free states. The starting and the goal position are denoted with an orange and a brown dot, respectively. Although the workspace looks trivial, the configuration space is irregular, which makes the planning difficult.

B More Preliminaries

Tree-based sampling planner The tree-based sampling planner algorithm is illustrated in Figure 9. The `Expand` in Algorithm 1 operator returns an existing node in the tree $s_{parent} \in \mathcal{V}$ and a new state $s_{new} \in \mathcal{S}$ sampled from the neighborhood of s_{parent}. Then the line segment $[s_{parent}, s_{new}]$ is passed to function `ObstacleFree` for collision checking. If the line segment $[s_{parent}, s_{new}]$ is collision-free (no obstacle in the middle, or called **reachable** from $\mathcal{T}$), then s_{new} is added to the tree vertex set $\mathcal{V}$, and the line segment is added to the tree edge set $\mathcal{E}$. If the newly added node s_{new} has reached the target $\mathcal{S}_{goal}$, the algorithm will return. Optionally, some concrete algorithms can define a `Postprocess` operator to refine the search tree. For an example of the `Expand` operator, as shown in Figure 1 (c), since there is no obstacle on the dotted edge $[s_{parent}, s_{new}]$, *i.e.*, s_{new} is reachable, the new state and edge will be added to the search tree (connected by the solid edges).

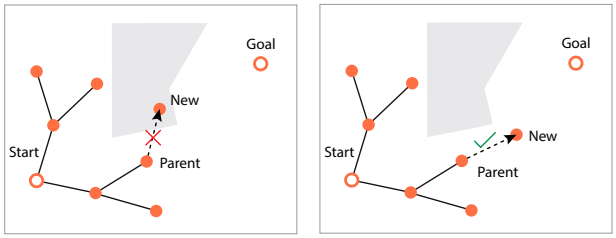

Figure 9: Illustration for one iteration of Algorithm 1. The left and right figures illustrate two different cases where the sample returned by the `Expand` operator is **unreachable** and **reachable** from the search tree.

Now we will provide two concrete algorithm examples. For instance,

- If we instantiate the `Expand` operator as Algorithm 4, then we obtain the rapidly-exploring random trees (RRT) algorithm (LaValle, 1998), which first samples a state s from the configuration space

Algorithm 4: RRT :: Expand$(\mathcal{T}, U)$

Data: $\mathcal{T} = (\mathcal{V}, \mathcal{E}), U = (s_{init}, \mathcal{S}_{goal}, \mathcal{S}, \mathcal{S}_{free}, \texttt{map}, c(\cdot))$

$s_{rand} \leftarrow \mathcal{U}nif(\mathcal{S})$; ▷ Sample configuration space

$s_{parent} \leftarrow \text{argmin}_{s \in \mathcal{V}} \|s_{rand} - s\|$; ▷ Pull to a tree node

$s_{new} \leftarrow \text{argmin}_{s \in \mathcal{B}(s_{parent}, \eta)} \|s - s_{rand}\|$;

return s_{parent}, s_{new};

Algorithm 5: EST :: Expand$(\mathcal{T}, U)$

Data: $\mathcal{T} = (\mathcal{V}, \mathcal{E}), U = (s_{init}, \mathcal{S}_{goal}, \mathcal{S}, \mathcal{S}_{free}, \texttt{map}, c(\cdot))$

$s_{parent} \sim \phi(s), s \in \mathcal{V}$; ▷ Sample a tree node

$s_{new} \leftarrow \mathcal{U}nif(\mathcal{B}(s_{parent}))$; ▷ Sample neighborhood

return $s_{nearest}, s_{new}$;

$\mathcal{S}$ and then pulls it toward the neighborhood of current tree $\mathcal{T}$ measured by a ball of radius η:

$$\mathcal{B}(s, \eta) = \{s' \in \mathcal{S} \mid \|s' - s\| \leqslant \eta\}.$$

Moreover, if the Postprocess operator is introduced to modify the maintained search tree as in RRT* (Karaman & Frazzoli, 2011), the algorithm is provable to obtain the optimal path asymptotically.

- If we instantiate the Expand operator as Algorithm 5, then we obtain the expansive-space trees (EST) algorithm (Hsu et al., 1997; Phillips et al., 2004), which samples a state s from the nodes of the existing tree, and then draw a sample from the neighborhood of s.

UCB-based algorithms Specifically, in a K-armed bandit problem, the UCB algorithm will first play each of the arms once, and then keep track of the average reward $\bar{r}_i$ and the visitation count n_i for each arm. After T rounds of trials, the UCB algorithm will maintain a set of information $\{(\bar{r}_i, n_i)\}_{i=1}^K$ with $\sum_{i=1}^K n_i = T$. Then, for the next round, the UCB algorithm will select the next arm based on the one-sided confidence interval estimation provided by the Chernoff-Hoeffding bound,

$$a^*_{T+1} = \text{argmax}_{i \in \{1, \ldots, K\}} \bar{r}_i + \lambda \sqrt{\frac{\log T}{n_i}}, \tag{7}$$

where λ controls the exploration-exploration trade-off. It has been shown that the UCB algorithm achieves $\mathcal{O}(\log T)$ regret. However, the MCTS is not directly applicable to continuous state-action spaces.

There have been many attempts to generalize the UCB and UCT algorithms to continuous state-action spaces (Chu et al., 2011; Krause & Ong, 2011; Couëtoux et al., 2011; Yee et al., 2016). For instance, contextual bandit algorithms allow continuous arms but involve a non-trivial high dimensional non-convex optimization to select the next arm. In UCT, the progressive widening technique has been designed to deal with continuous actions (Wang et al., 2009). Even with these extensions, the MCTS restricts the exploration only from leaves states, implicitly adding an unnecessary hierarchical structure for path planning, resulting inferior exploration efficiency and extra computation in path planning tasks.

Although these off-the-shelf algorithms are not directly applicable to our path planning setting, their successes show the importance of exploration-exploitation trade-off and will provide the principles for our algorithm for continuous state-action planning problems.

Planning networks Value iteration networks (Tamar et al., 2016) employ neural networks to embed the value iteration algorithm from planning and then use this embedded algorithm to extract input features and define downstream models such as value functions and policies.

Specifically, VIN mimics the following recursive application of Bellman update operator $\mathcal{G}$ to value function V^*,

$$V^*(s|U) = (\mathcal{G}V^*)(s) := \min_a \sum_{s'} P(s'|s, a)(c([s, s']) + V^*(s'|U)). \tag{8}$$

where $P(s'|s, a)$ is the state transition model. When the state space for s and action space for a are low dimensional, these spaces can be discretized into grids. Then, the local cost function $c([s, s'])$ and the

value function $V^*(s'|U)$ can be represented as matrices (2d) or tensors (3d) with each entry indexed by grid locations. Furthermore, if the transition model $P(s'|s,a)$ is local, that is $P(s'|s,a) = 0$ for $s' \notin \mathcal{B}(s)$, it resembles a set of convolution kernels, each indexed by a discrete action a. And the Bellman update operator essentially convolves $P(s'|s,a)$ with $c([s,s'])$ and $V^*(s'|U)$, and then performs a $\min$-pooling operation across the convolution channels.

Inspired by the above computation pattern of the Bellman operator, value iteration networks design the neural architecture as follows,

$$\tilde{V}^{*0} = \min \left(W_1 \oplus \left[\texttt{map}, \tilde{R} \right] \right) \tag{9}$$

$$\tilde{V}^{*t} = \min \left(W_1 \oplus \left[\tilde{V}^{*t-1}, \tilde{R} \right] \right) \tag{10}$$

where $\oplus$ is the convolution operation, both $\texttt{map}$, $\tilde{V}^{*t}$ and $\tilde{R}$ are $d \times d$ matrices, and the parameter W_1 are k_c convolution kernels of size $k \times k$. The $\min$ implements the pooling across k_c convolution channels.

The gated path planning networks (GPPN) (Lee et al., 2018) improves the VIN by replacing the VIN cell (9) with the well-established LSTM update, *i.e.*,

$$\tilde{V}^t, \tilde{c}^t = \texttt{LSTM} \left(\sum \left(W_1 \oplus \left[\tilde{V}^t, \tilde{R} \right] \right), \tilde{c}^t \right), \tag{11}$$

where the summation is taking over all the k_c convolution channels.

After constructing the VIN and GPPN, the parameters of the model, *i.e.*, $\left\{ \tilde{R}, W_1 \right\}$ can be learned by imitation learning or reinforcement learning.

The application of planning networks are restricted in low-dimension tasks. However, their success enlightens our neural architecture for generalizable representation for high-dimension planning tasks.

C Parametrized UCB Algorithms

We list two examples of parametrized UCB as the instantiation of (3) used in GPE:

- **GP-UCB**: The GP-UCB Chu et al. (2011) is derived by parameterizing via Gaussian Processes (GP) with kernel $k(s,s')$, *i.e.*, $\mathbb{E}[r(s)|\mathcal{T},U] \sim \mathcal{GP}(0,k)$, GP-UCB maintains an UCB of the reward after t-step as
$$\phi(s) := \bar{r}_t(s) + \lambda \sigma_t(s), \tag{12}$$
where
$$\begin{aligned} \bar{r}_t(s) &= k_t(s) (K_t + \alpha I)^{-1} r_t, \\ \sigma_t^2(s) &= k(s,s) - k_t(s)^\top (K_t + \alpha I)^{-1} k_t(s), \end{aligned}$$
with $k_t(s) = [k(s_i,s)]_{s_i \in \mathcal{S}_t}$, $K_t = [k(s,s')]_{s,s' \in \mathcal{S}_t}$, and $\mathcal{S}_t = \{s_1, s_2, \ldots, s_t\}$ denotes the sequence of selected nodes in current trees. The variance estimation $\sigma_t^2(s)$ takes the number of visits into account in an implicit way: the variance will reduce, as the neighborhood of s is visited more frequently (Srinivas et al., 2009).

- **KS-UCB**: We can also use kernel regression as an alternative parametrization for (7) (Yee et al., 2016), which leads to an UCB of the reward after t-step as
$$\phi(s) := \bar{r}_t(s) + \lambda \sigma_t(s), \tag{13}$$
where
$$\begin{aligned} \bar{r}_t[s] &= \frac{\sum_{s' \in \mathcal{S}_t} k(s',s) r(s')}{\sum_{s' \in \mathcal{S}_t} k(s',s)}, \\ \sigma_t(s) &= \sqrt{\frac{\log \sum_{s' \in \mathcal{S}_t} w(s')}{w(s)}}, \end{aligned}$$
with $w(s) = \sum_{s' \in \mathcal{S}_t} k(s',s)$. Clearly, the variance estimation is to promote exploration towards less frequently visited states.

As we can see, in both two examples of the parametrized UCB, we parametrize the observed rewards, leading to generalizable UCB for increased states by considering the correlations.

D POLICY AND VALUE NETWORK ARCHITECTURE

We explain the implementation details of the proposed parametrization for policy and value function. Figure 10 and Figure 11 are neural architectures for the attention module, the policy/value network, and the planning module, respectively.

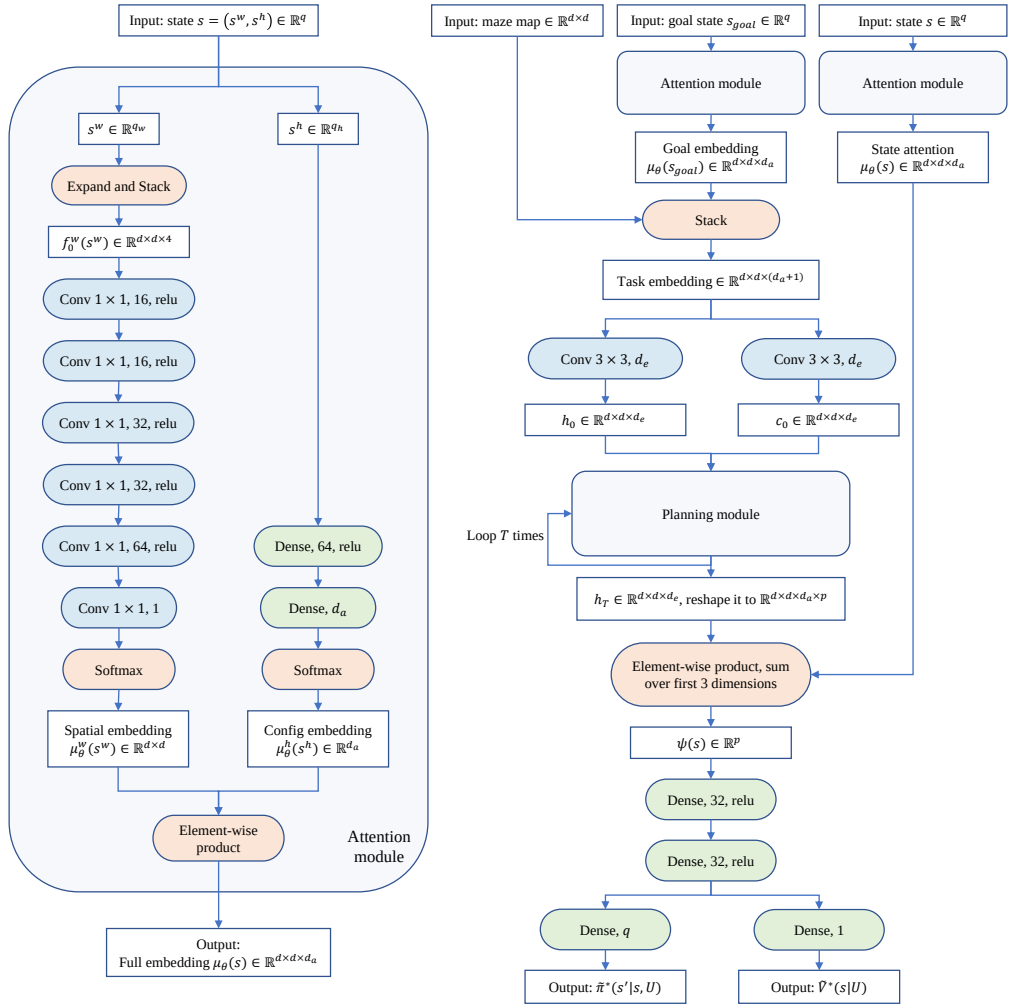

Figure 10: Left: attention module, instantiating the Figure 3; Right: policy/value network, instantiating the Figure 4.

In the figures, we use rectangle blocks to denote inputs, intermediate results and outputs, stadium shape blocks to denote operations, and rounded rectangle blocks to denote modules. We use different colors for different operations. In particular, we use blue for convolutional/LSTM layers, green for dense layers, and orange for anything else. For convolutional layers, "Conv 1×1, 32, relu" denotes a layer with 1×1 kernels, 32 channels, followed by a rectified linear unit; for dense layers, "Dense, 64, relu" denotes a layer of size 64, followed by a rectified linear unit.

The attention module (Figure 10-left) embeds a state to a $d \times d \times d_a$ tensor. The planning module (Figure 11) is a one-step LSTM update which takes the result of a convolutional layer as input. Both the input and hidden size of the LSTM cell are d_e. All $d \times d$ locations share one set of parameters and are processed by the LSTM in one batch.

The main architecture is illustrated in Figure 10-right. It takes maze map, state and goal as input, and outputs the action and the value. Refer to Section 4.2 for details for computing $\psi(s)$. In our experiments, we set the values of the hyper-parameters to be $(d, d_e, d_a, p) = (15, 64, 8, 8)$.

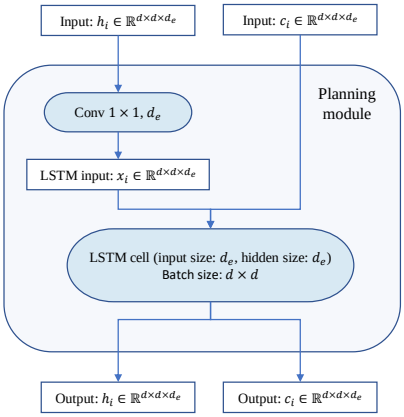

Figure 11: planning module

E Experiment Details

E.1 Benchmark Environments

We used four benchmark environments in our experiment. For the first three, the workspace dimension is 2d. We generated the maze maps with the recursive backtracker algorithm using the following implementation: https://github.com/lileee/gated-path-planning-networks/blob/master/generate_dataset.py. Examples of the workspace are shown in Figure 13. Three environments differ in the choice of robots:

- **Workspace planning (2d).** The robot is abstracted with a point mass moving in the plane. Without higher dimensions, this problem reduces to planning in the workspace.
- **Rigid body navigation (3d).** A rigid body robot, abstracted as a thin rectangle, is used here. The extra rotation dimension is added to the planning problem. This robot can rotate and move freely without any constraints in the free space.
- **3-link snake (5d).** The robot is a 5 DoF snake with two joints. Two more angle dimensions are added to the planning task. To prevent links from folding, we restrict the angles to the range of $[-\pi/4, \pi/4]$.

The fourth environment has a 3d workspace. Cuboid obstacles were generated uniformly randomly in space with density $\approx 20\%$. Example of the workspace is shown in Figure 6 and 14, where the blue cuboids are obstacles. The environment is described below:

- **Spacecraft planning (7d).** The robot is a spacecraft with a cuboid body and two 2 DoF arms connecting to two opposite sides of the body. There is a joint in the middle of each arm. The outer arm can rotate around this joint. Each arm can also rotate as a whole around its connection point with the body. All rotation angles are restricted in the range of $[0, \pi/2]$. The spacecraft itself cannot rotate.

E.2 Hyperparameter for MSIL

During self-improving over the first 2000 problems, NEXT updated its parameters and annealed ϵ once for every 200 problems. The value of the annealing ϵ was set as the following:

$$\epsilon = \begin{cases} 1, & \text{if } i < 1000, \\ 0.5 - 0.1 \cdot \lfloor (i - 1000)/200 \rfloor, & \text{if } 1000 \leqslant i < 2000, \\ 0.1, & \text{otherwise,} \end{cases}$$

with i denoting the problem number.

E.3 Baseline: the Improved GPPN

The original GPPN is not directly applicable to our experiments. Inspired by Tamar et al. (2016), we add a fully-connected MLP to its final layers, so that the improved architecture can be applied to high-dimensional continuous domain. As shown in Figure 12, the GPPN first processes the discretized

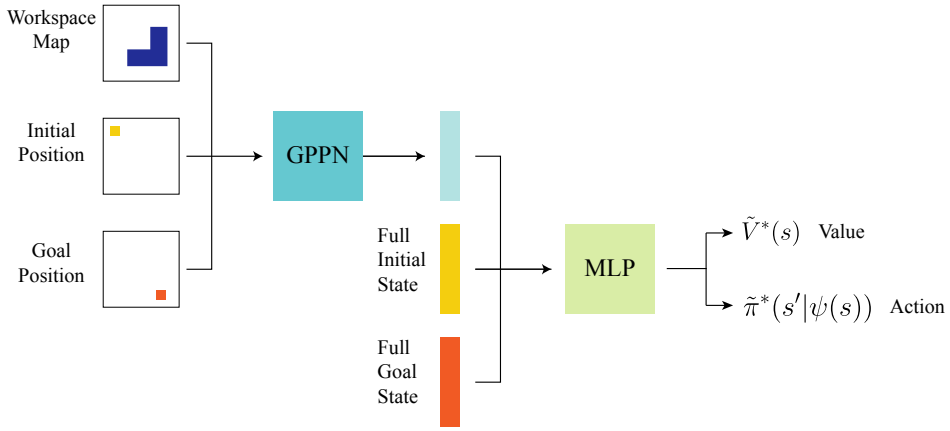

Figure 12: Improved GPPN architecture

workspace locations. Its output and the full robot configurations are processed together by the MLP, which then produces the current value and action estimates. The improved GPPN is trained using supervisions from the near-optimal paths produced by RRT*.

F Experiment Results

F.1 Solution Path Illustration

Figure 13: The solution path produced by NEXT in a workspace planning task (2d), rigid body navigation task (3d), 3-link snake task (5d) from left to right. The orange dot and the brown dot are starting and goal locations, respectively.

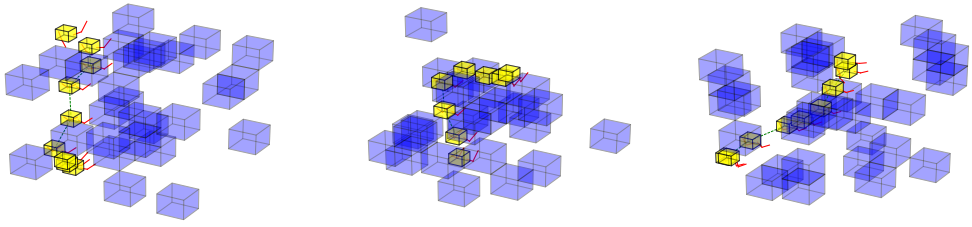

Figure 14: The solution paths produced by NEXT in spacecraft planning task (7d). Spacecraft has a yellow body and two 2 DoF (red) arms. Blue cuboids are obstacles.

F.2 Details of Quantitative Evaluation

More detailed results are shown in Table 1, 2, 3, including learning-based and non-learning-based ones, on the last 1000 problems in each experiment. We normalized the number of collision checks and the cost of paths based on the solution of RRT*. The success rate result is not normalized. The

best planners in each experiment are in **bold**. NEXT-KS and NEXT-GP outperform the current state-of-the-art planning algorithm with large margins.

Table 1: Success rate results. The higher the better. NEXT-KS performs the best.

	NEXT-KS	NEXT-GP	GPPN-KS	GPPN-GP	RRT*	BIT*	BFS	CVAE	Reject
2d	**0.988**	0.981	0.718	0.632	0.735	0.710	0.185	0.535	0.720
3d	**0.943**	0.841	0.689	0.554	0.490	0.514	0.121	0.114	0.498
5d	**0.883**	0.768	0.633	0.515	0.455	0.497	0.030	0.476	0.444
7d	**0.931**	0.906	0.634	0.369	0.361	0.814	0.288	0.272	0.370

Table 2: Average number of collision checks results. The lower the better. The score is normalized based on the solution of RRT*. NEXT-KS performs the best in 3 benchmarks.

	NEXT-KS	NEXT-GP	GPPN-KS	GPPN-GP	RRT*	BIT*	BFS	CVAE	Reject
2d	**0.177**	0.243	2.342	3.484	1.000	5.945	9.247	1.983	1.011
3d	**0.694**	1.334	2.214	3.125	1.000	7.924	7.292	2.162	0.988
5d	**0.888**	1.520	1.800	2.706	1.000	7.483	5.758	1.188	0.997
7d	0.653	**0.502**	1.877	1.313	1.000	4.683	3.856	1.591	0.987

Table 3: Average cost of paths. The lower the better. The score is normalized based on the solution of RRT*. The NEXT-KS achieves the best solutions.

	NEXT-KS	NEXT-GP	GPPN-KS	GPPN-GP	RRT*	BIT*	BFS	CVAE	Reject
2d	**0.172**	0.193	1.049	1.333	1.000	1.140	2.811	1.649	1.050
3d	**0.116**	0.315	0.612	0.875	1.000	0.955	1.720	1.734	0.984
5d	**0.215**	0.426	0.673	0.890	1.000	0.923	1.780	0.961	1.020
7d	**0.108**	0.147	0.573	0.987	1.000	0.291	1.114	1.139	0.986

We demonstrated the performance improvement curves for 2d workspace planning, 3d rigid body navigation in Figure 15. As we can see, similar to the performances on 5d 3-link snake planning task in Figure 7, in these tasks, the NEXT-KS and NEXT-GP improve the performances along with more and more experiences collected, justified the self-improvement ability by learning $\tilde{V}^*$ and $\tilde{\pi}^*$.

F.3 Search Trees Comparison

We illustrate the search trees generated by RRT* and the proposed NEXT algorithms with 500 samples in Figure 16, Figure 17, Figure 18 and Figure 19 on several 2d, 3d, 5d and 7d planning tasks, respectively. To help readers better understand how the trees were expanded, we actually visualize the RRT* search trees without edge rewiring, which is equivalent to the RRT search trees, however the vertex set is the same. Comparing to the search trees generated by RRT* side by side, we can clearly see the advantages and the efficiency of the proposed NEXT algorithms. In all the tasks, even in 2d workspace planning task, the RRT* indeed randomly searches without realizing the goals, and thus cannot complete the missions, while the NEXT algorithms search towards the goals with the guidance from $\tilde{V}^*$ and $\tilde{\pi}^*$, therefore, successfully provides high-quality solutions.

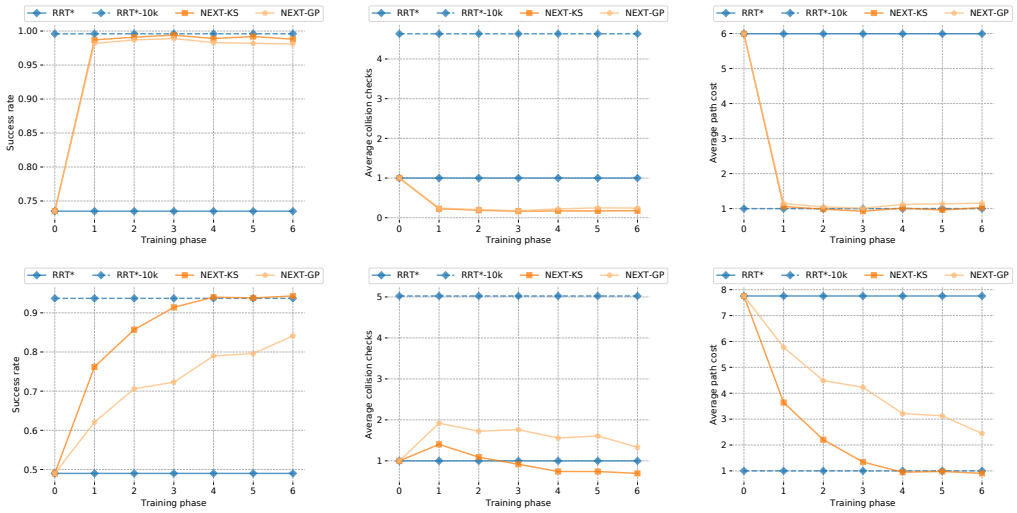

Figure 15: The first and second rows display the improvement curves of our algorithms on all 3000 problems of the 2d workspace planning and 3d rigid body navigation problems. We compare our algorithms with RRT*. Three columns correspond to the success rate, the average collision checks, and the average cost of the solution paths for each algorithm.

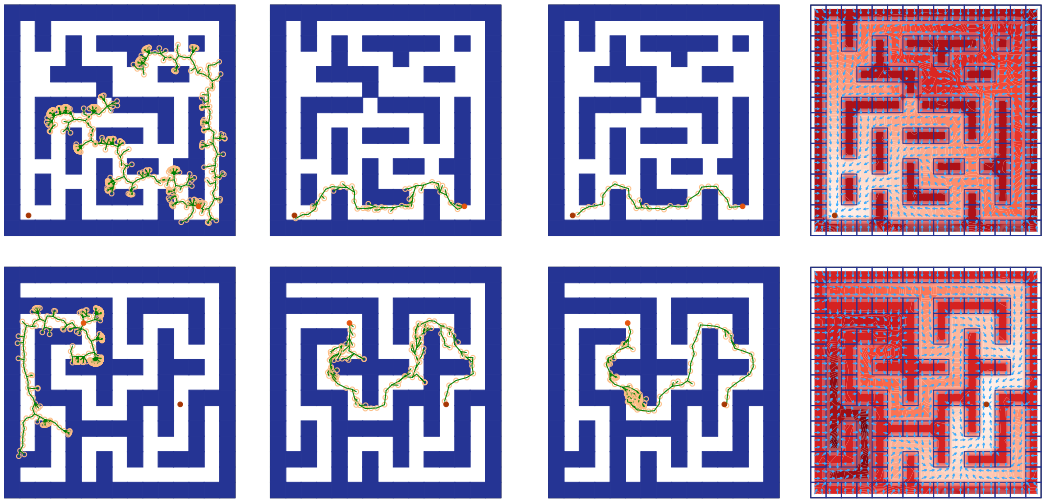

(a) RRT* (w/o rewiring) (b) NEXT-KS search tree (c) NEXT-GP search tree (d) learned $\tilde{V}^*$ and $\tilde{\pi}^*$

Figure 16: Column (a) to (c) are the search trees produced by the RRT*, NEXT-KS, and NEXT-GP on the same workspace planning task (2d). The learned $\tilde{V}^*$ and $\tilde{\pi}^*$ from NEXT-KS are plotted in column (d). In the figures, obstacles are colored in deep blue, the starting and goal locations are denoted by orange and brown dots, respectively. In column (a) to (c), samples are represented with hollow yellow circles, and edges are colored in green. In column (d), the level of redness denotes the value of the cost-to-go estimate $\tilde{V}^*$, and the cyan arrows point from a given state s to the center of the proposal distribution $\tilde{\pi}^*(s'|s, U)$. We set the maximum number of samples to be 500.

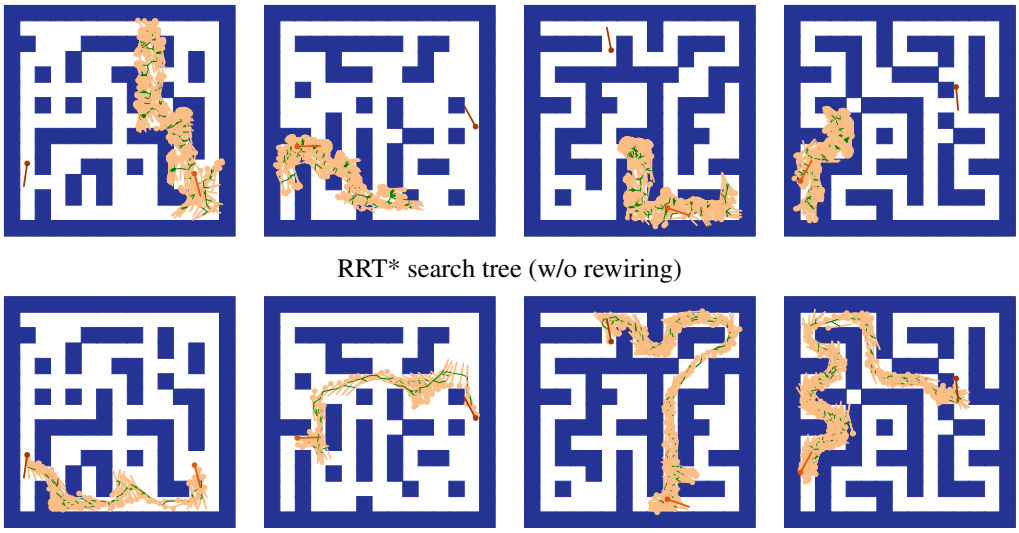

RRT* search tree (w/o rewiring)

NEXT-KS search trees

Figure 17: Each column corresponds to one example from the rigid body navigation problem (3d). The top and the bottom rows are the search trees produced by the RRT* and NEXT-KS, respectively. In the figures, obstacles are colored in deep blue, and the rigid bodies are represented with matchsticks. The samples, starting states, and goal states are denoted by yellow, orange, and brown matchsticks, respectively. Edges are colored in green. We set the maximum number of samples to be 500.

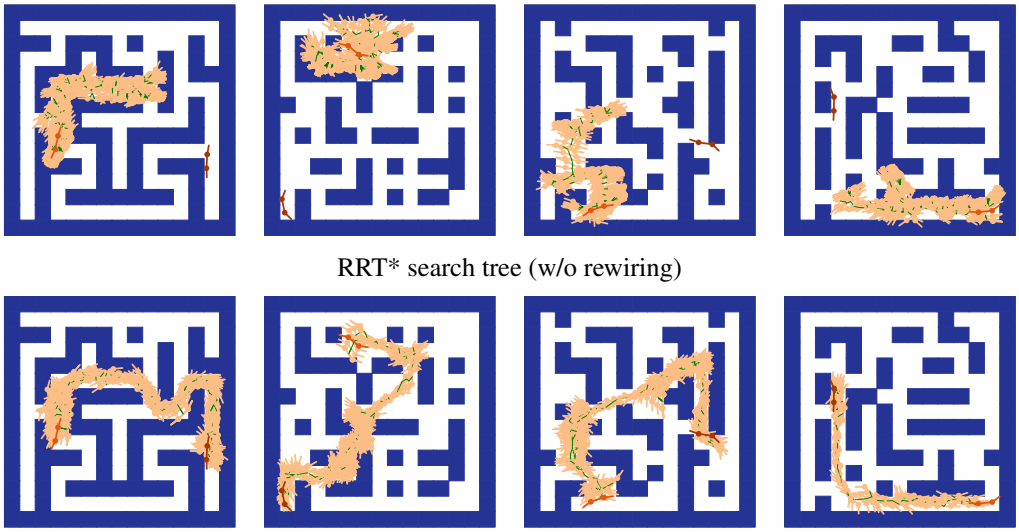

RRT* search tree (w/o rewiring)

NEXT-KS search trees

Figure 18: Each column corresponds to one example from the 3-link snake problem (5d). The top and the bottom rows are the search trees produced by the RRT* and NEXT-KS, respectively. In the figures, obstacles are colored in deep blue, and the rigid bodies are represented with matchsticks. The samples, starting states, and goal states are denoted by yellow, orange, and brown matchsticks, respectively. Edges are colored in green. We set the maximum number of samples to be 500.

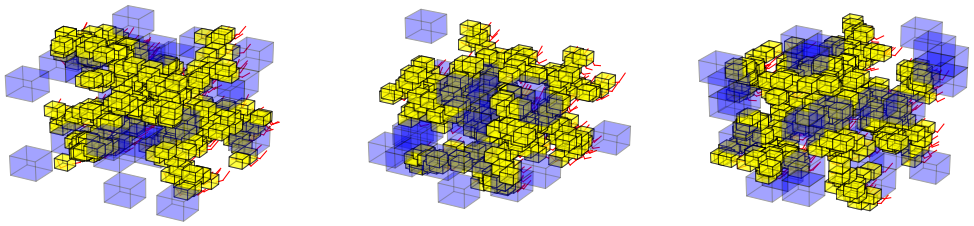

RRT* search tree (w/o rewiring)

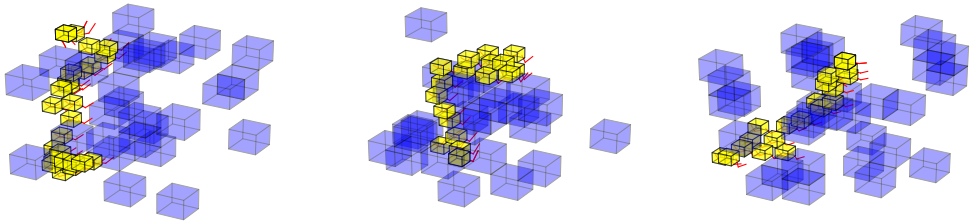

NEXT-KS search trees

Figure 19: Each column corresponds to one example from the spacecraft planning problem (7d). The top and the bottom rows are the search trees produced by the RRT* and NEXT-KS, respectively. In the figures, obstacles are colored in blue, and each spacecraft has a yellow body and two 2 DoF red arms. We set the maximum number of samples to be 500.